

# Modeling global anthropogenic erosion in the Holocene

The Holocene  
2019, Vol. 29(3) 367–379  
© The Author(s) 2018  
Article reuse guidelines:  
sagepub.com/journals-permissions  
DOI: 10.1177/0959683618816499  
journals.sagepub.com/home/hol  


Zhengang Wang<sup>1,2</sup> and Kristof Van Oost<sup>2</sup>

## Abstract

A large proportion of natural vegetation has been converted to agricultural use, and this typically accelerates erosion by one to two orders of magnitude. Quantification of this accelerated erosion is important to understand the impact of human activities on soil ecosystem service given that soil erosion induces soil degradation and changes in soil organic carbon (SOC) stocks. Until now, few studies have evaluated the accumulated impact of agricultural erosion, since the start of agriculture (ca. 6000 BC), on the soils system and the carbon cycle. In this study, we mainly focused on the enhanced water erosion by conversion of natural vegetation to crops, while wind erosion on the cropland is not assessed. We first evaluated and constrained existing anthropogenic land cover change (ALCC) scenarios by comparing observed cumulative erosion for the agricultural period under a wide range of global agro-ecological conditions with model simulations. An optimized land-use scenario that makes the best fit between the simulation and the observation was derived in the model calibration. We further applied a spatially distributed erosion model, which was modified based on Revised Universal Soil Loss Equation (RUSLE), under the optimized land-use scenario across globe to estimate the total anthropogenic cumulative erosion and characterize their spatial variability. Simulations suggest that conversion from natural vegetation to cropland has caused a global cumulative agricultural erosion of  $27,187 \pm 9030$  Pg for the period of agriculture. This results in an average cumulative sediment mobilization of  $1829 \pm 613$  kg m<sup>-2</sup> on croplands, corresponding to a soil truncation of ca.  $1.34 \pm 0.45$  m. Regions of early civilization, particularly with high cropland fractions such as South Asia, Southeast Asia, and Central America have higher area-averaged anthropogenic erosion than other regions. This results in spatial variability in soil truncation rates because of erosion, which would further affect the soil production rate. Our study shows that observations of long-term anthropogenic erosion at the catchment scale can be used to constrain the reconstructed land-use scenarios.

## Keywords

anthropogenic erosion, Holocene, land-use scenario, modeling

Received 18 November 2017; revised manuscript accepted 8 October 2018

## Introduction

Humans are altering the Earth system at increasing rates (Ruddiman, 2007; Waters et al., 2016). One of the main agents of this anthropogenic disturbance is the clearance of woody vegetation. This anthropogenic land cover change (ALCC) imposes substantial impacts on the Earth system. ALCC has resulted in significant terrestrial biodiversity loss through habitat conversion and degradation (e.g. Murphy and Romanuk, 2014; Newbold et al., 2015), while emissions from ALCC are one of the largest anthropogenic sources of atmospheric CO<sub>2</sub>. ALCC is now considered as the most uncertain component of both the past and present global C cycle (Houghton et al., 2012; Kaplan et al., 2011; Pongratz et al., 2009; Stocker et al., 2011).

It is also well known that conversion of natural land cover for agriculture accelerates soil erosion by one to two orders of magnitude (Montgomery, 2007; Vanacker et al., 2007). This accelerated soil erosion not only causes serious onsite soil degradation (Bakker et al., 2007; Montgomery, 2007), but it also has detrimental effects on water quality (Heinz et al., 2015; Muenich et al., 2016). Furthermore, soil erosion and sediment deposition reshape the landscape and supply sediments to the fluvial systems (Rommens et al., 2007; Trimble, 1999). Soil redistribution by erosion causes spatial variability of soil depth, thereby imposing an impact on the soil production rate (Heimsath et al., 1997; Yoo et al., 2009). The redistribution of soil organic carbon (SOC) associated with the eroded sediments also has a significant impact

on carbon cycling (Harden et al., 1999; Stallard, 1998). Studies have reported that this redistribution has a significant impact on the contemporary global C cycle and the climate system (Chappell et al., 2016; Quinton et al., 2010; Yue et al., 2016). However, most studies have focused on relatively short timescales, ranging from single erosion events to several decades (e.g. Van Oost et al., 2007). In contrast, little is known about the effects of ALCC, and the associated accelerated erosion, on the net exchange of C between the terrestrial ecosystem and the atmosphere since the start of agricultural activities ca. 8000 years ago. At present, a comprehensive assessment is lacking of how accelerated erosion has evolved during the agricultural period at the global scale, and particularly the spatial distribution of erosion.

At the catchment scale, extensive studies have been performed to investigate the impact of ALCC on long-term erosion processes in various environments spanning from recent centuries (Beach, 1994; Trimble, 1981) to the whole Holocene (Anselmetti et al.,

<sup>1</sup>School of Geography and Planning, Sun Yat-Sen University, China

<sup>2</sup>Georges Lemaître Center for Earth and Climate Research (TECLIM), Earth and Life Institute, Université catholique de Louvain, Belgium

## Corresponding author:

Zhengang Wang, School of Geography and Planning, Sun Yat-Sen University, Guangzhou 510275, China.

Email: wangzhg33@mail.sysu.edu.cn

2007; Hoffmann et al., 2013). A number of studies derived long-term erosion rates by identifying sediment stages in colluvial and alluvial deposits. This is typically done using OSL dating or  $^{14}\text{C}$  dating with buried charcoals to obtain the temporal variation (Fuchs et al., 2011; Houben, 2012; Rommens et al., 2007; Wolf and Faust, 2013). Other studies have focused on lacustrine sediment archives in hydrologically closed catchments (Dearing et al., 1987; Enters et al., 2008; O'Hara et al., 1993; Oldfield et al., 2003). The depth of soil truncation, by comparing eroding soil profiles within non-eroded reference profiles, has also been used (Ciampalini et al., 2012; Rommens et al., 2005). At the global scale, Wilkinson and McElroy (2007) presented the first estimate of cumulative erosion related to agriculture; they estimated that ca. 20,000 Pg of soil has been eroded through the history of civilization. This estimate is based on the temporal evolution of per capita mass of soil displaced through agricultural and construction practices (Hooke, 2000; Wilkinson and McElroy, 2007). This initial work provided a first, but spatially lumped, estimation of the order of magnitude. However, information on the spatial variation of cumulative erosion would be helpful to understand relevant controlling factors and to identify regions of severe erosion.

Previous studies have reconstructed spatially explicit scenarios of historical land use, for example, HYDE (Klein Goldewijk et al., 2010, 2011) and KK10 (Kaplan et al., 2011). However, because of the fact that reliable information on land use is not available everywhere, existing land-use reconstruction scenarios are mainly based on estimations of past population densities and on assumptions on how people used the land. The differences in the relationships used between population and cropland area result in large discrepancies between land-use scenarios. For instance, at the early phases of civilization, the KK10 land-use scenario is characterized by a much larger area occupied by cropland when compared with the HYDE scenario. This is an important issue given that the cumulative agricultural erosion integrates changes in cropland area and average erosion over time. HYDE and KK10 land-use scenarios will hence result in very different estimates of agricultural soil erosion throughout the Holocene. Here we contend that, observational data on long-term erosion at the catchment scale provide new insights into the robustness of the reconstructed land-use scenarios by comparing the measured cumulative erosion with simulations based on these land-use scenarios.

In this study, we performed a literature review and extracted observations on catchment-scale anthropogenic erosion from published studies that cover the whole agricultural period. We modified a global and spatially explicit erosion model (Van Oost et al., 2007) that is capable of representing the temporal variation of erosion at long timescales (i.e. millennial). Our objectives are to (1) evaluate and constrain two contrasting ALCC scenarios, that is, HYDE and KK10 scenarios by calibrating and validating the modified erosion model at catchments where model-testing data is available and (2) use the validated model to estimate total anthropogenic cumulative erosion and to characterize their spatial variability by applying the model across the globe. The framework used here was developed as part of a previous study (Wang et al., 2017). In this manuscript, we substantially enlarged the scope of the study by adding the following components:

1. More observations derived from the literature were added for the model calibration. This should result in a more robust estimation of the parameter values.
2. In Wang et al. (2017), the model was spatially lumped with only a differentiation in relation to four Köppen climate zones. Here, a fully spatially explicit model is presented and applied globally at a resolution of 5 arc minutes.

3. In addition to the estimation of cumulative anthropogenic sediment volumes, we also present and analyze the spatial variability of the sediment ages here, as this is an important metric for carbon stabilization.

## Materials and methods

### Sites and field data

We performed a literature review to find empirical studies on human-induced erosion at the catchment scale. We selected those studies that report on the whole agricultural period, that is, from the start of cultivation to present-day, and which provide information at large spatial scales, so that the observations are compatible with the scale of our model. To the best of our knowledge, a limited number of studies fitted these criteria. In total, we obtained 14 studies that report on empirical measurements from different continents with different climate and agricultural histories (Figure 1).

The measurements of long-term anthropogenic erosion of these 14 catchments were derived from different methods. In the enclosed catchments discharging into lakes, the long-term anthropogenic erosion was obtained by estimating sediment deposition in lakes (Anselmetti et al., 2007; Dearing et al., 1987; Enters et al., 2008; O'Hara et al., 1993). Given that these data were collected from small catchments in hilly regions, sediments stored at the footslope as colluvia before reaching lakes are very limited. The sediments deposited in lakes were therefore regarded as the total erosion of the catchments. In the other catchments, the erosion was obtained via application of Universal Soil Loss Equation (USLE) model or field surveys on soil truncation and sediment storage in colluvia and alluvia (Beach, 1994; Houben, 2012; Trimble, 1981; van Hooff and Jungerius, 1984; Van Oost et al., 2012). For catchments with only observations on sediment storage in colluvial and alluvial settings (Hoffmann et al., 2013; Saito et al., 2001), the cumulative erosion was derived by assigning sediment delivery ratios. Given that sediment delivery ratios vary with time (Hoffmann, 2015) and that they also are affected by factors such as catchment area and topography (de Vente et al., 2007), we utilized a Monte Carlo approach to account for the variability of sediment delivery ratios (see below for the application of Monte Carlo simulation). The range of the sediment delivery ratios was derived from a compilation of field observation (Hoffmann, 2015). The Yellow River catchment data is a particular case as subsoil erosion (i.e. from gully and landsliding) plays an important role here (Zhao et al., 2016). Separation between topsoil erosion and subsoil erosion was needed because our model only considers anthropogenic sediment generation in the upper layer of the soil profile, while subsoil erosion is mainly caused by natural processes. Thus, the observed total cumulative sediment of the Yellow River catchment was divided into topsoil and subsoil sediments. Analysis on field measurements shows that topsoil erosion represents about half of the total erosion in the Yellow River catchment (Zhao et al., 2016). The measurements of long-term anthropogenic erosion are listed in Table 1.

### Soil erosion

In this study, we mainly focused on the enhanced water erosion by conversion of natural vegetation to crops, while wind erosion on the cropland is not assessed. We only considered the mobilized soils on croplands by interrill and rill erosion, because this is closely related to the in situ soil degradation and soil properties. The consequent sediment deposition in colluvial and alluvial settings and delivery in river systems were not taken into account, because it is more related to topography evolution and requires more information on geomorphology.

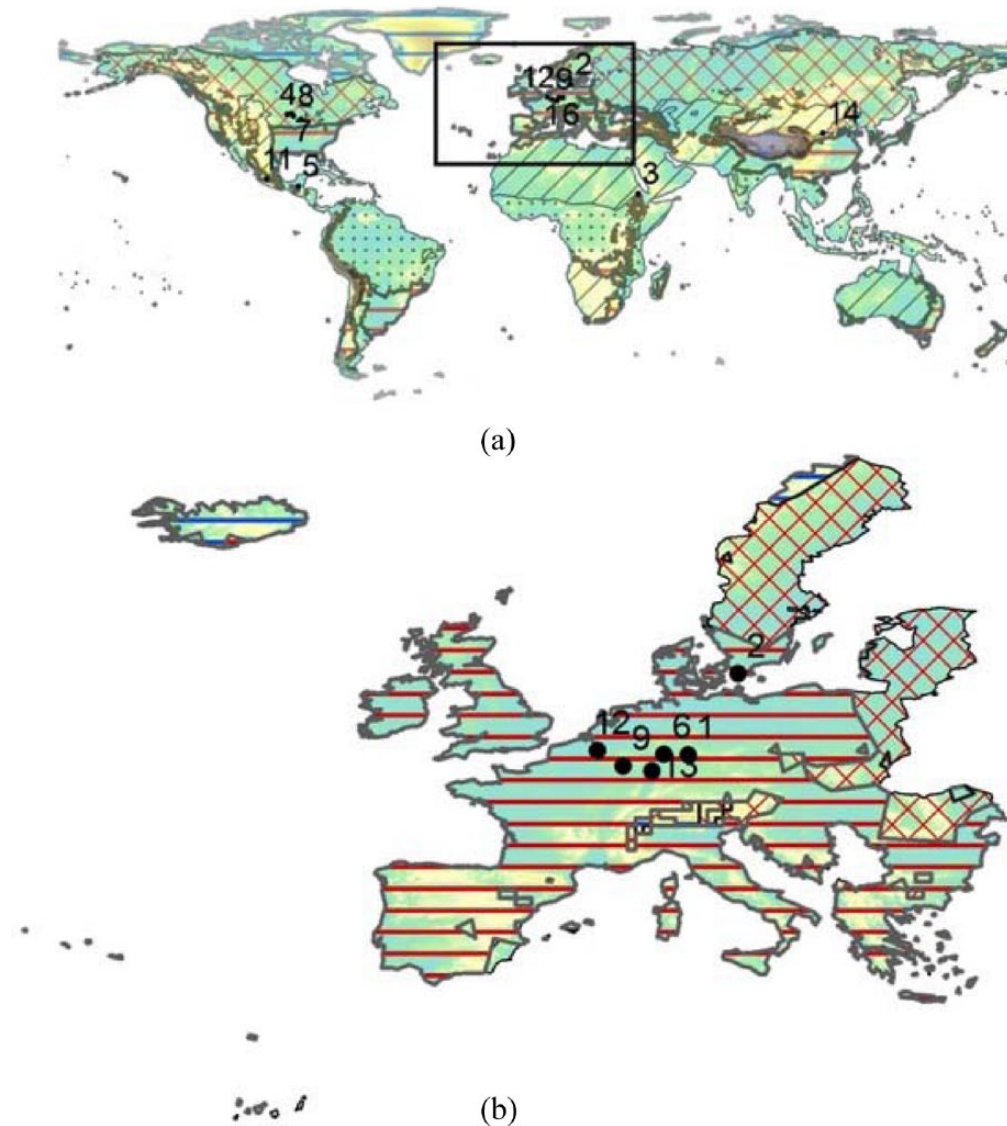


**Figure 1.** Locations of the catchments with measured anthropogenic sediments (a) all the catchments and (b) enlarged area showing the six catchments in Europe. The background color indicates elevation and the hatching indicates climatic zone based on Köppen climatic classification system (dots: tropical; slashed lines: dry; red horizontal lines: temperate; crossed lines: continental; blue horizontal lines: polar).

Present-day rates of cropland water erosion were estimated based on factors such as topography, land-use, and rainfall characteristics. The NRI is a statistical survey of land-use and natural resource conditions and trends on US non-Federal lands (NRCS, 2007). It reports the average soil losses in the US at the catchment scale. We used the NRI data to calibrate our model to ensure that the average erosion estimate for the US derived from global databases equals that from NRI observations. The estimation was performed across the globe. Analysis showed that soil erodibility, slope length, and management did not contribute much to explaining the variability in soil erosion at the catchment scale (Doetterl et al., 2012; Van Oost et al., 2007), and therefore, these factors were not included in the estimation of erosion. In our model, values of factors controlling soil losses are based on a reference condition. In this study, the mean of NRI data was used as the reference condition. This allows a robust estimation of the global mean soil losses. The variability of the NRI data was accounted for in a Monte Carlo approach (see below for details). For our global approach, we use the following equation based on RUSLE:

$$E = S_r \times R_r \times C_r \times E_r \quad (1)$$

where  $E$  is the estimated average soil loss per year on cultivated cropland by water erosion ( $\text{m yr}^{-1}$ ),  $S_r$  is the local slope factor

divided by the NRI derived mean for the US,  $R_r$  is the local rainfall erodibility factor divided by the NRI derived mean for the US,  $C_r$  is the local crop factor divided by the NRI derived mean for the US, and  $E_r$  is the average annual erosion for US cultivated cropland standardized to a slope of 9% ( $\text{m yr}^{-1}$ ). The spatial distribution of cropland for 1997 reconstructed by Klein Goldewijk et al. (2011) was used in this study. Details on the calculation of each erosion factor using global data and corrections using NRI data can be found in Van Oost et al. (2007) and Doetterl et al. (2012).

In our model, agricultural erosion occurs when land is used as cropland, and ceases when cropland is reconverted to non-cropland (the latter can occur when cropland area decreases over time). Given the fact that agricultural activities are preferably located on level areas, where soils typically have higher fertility and are easier to cultivate, flatter areas have a large likelihood to be converted into cropland during the early stages of agriculture. This implies that the average slope of the cropland increases with the increasing cropland area (Van Rompaey et al., 2001). This temporal variation of erosion (per unit area of cropland) was represented in our approach by linking the erosion to cropland area. We used present-day erosion by water as a baseline. Hence, we represented the erosion (per unit area of cropland) at the start of agriculture as a fraction of the present-day erosion (per unit area of cropland) as follows:

**Table 1.** Observed and simulated cumulative catchment-scale anthropogenic sediment fluxes.

No.	Reference	Catchment	Region	Koppen climate zone	Watershed area (km <sup>2</sup> )	Period	Observed cumulative sediments (g)	Simulated cumulative sediments (g)		This study
								HYDE	KK10	
1	Enters et al. (2008)	Frickenhauser See Lake catchment	Germany	Temperate	0.084	AD 600–2000	$4.33 \times 10^{10}$	$(7.89 \pm 1.56) \times 10^9$	$(3.77 \pm 1.12) \times 10^{11}$	$(1.06 \pm 0.51) \times 10^{11}$
2	Dearing et al. (1987)	Havardsson Lake catchment	Sweden	Temperate	0.86	3200 BC–AD 2000	$2.69 \times 10^{11}$	$(1.49 \pm 0.27) \times 10^{11}$	$(2.99 \pm 1.14) \times 10^{11}$	$(2.27 \pm 0.60) \times 10^{11}$
3	Ciampalini et al. (2012)	Aksum catchment	Ethiopia	Dry	1	40 BC–AD 2006	$5.19 \times 10^{11}$	$(3.0 \pm 0.58) \times 10^{10}$	$(1.3 \pm 0.43) \times 10^{12}$	$(5.0 \pm 0.15) \times 10^{11}$
4	Beach (1994)	Indian Creek catchment	USA	Continental	17	AD 1851–1988	$1.7 \times 10^{12}$	$(1.07 \pm 0.11) \times 10^{12}$	$(4.33 \pm 0.44) \times 10^{11}$	$(7.13 \pm 1.33) \times 10^{11}$
5	Anselmetti et al. (2007)	Salpeten Lake catchment	Guatemala	Tropical	3.81	6000 BC–AD 2000	$4.75 \times 10^{12}$	$(2.29 \pm 0.23) \times 10^{11}$	$(1.06 \pm 0.20) \times 10^{13}$	$(4.14 \pm 1.86) \times 10^{12}$
6	Houben (2012)	Rockenberg catchment	Germany	Temperate	10.24	3000 BC–AD 2000	$9.65 \times 10^{12}$	$(1.70 \pm 0.41) \times 10^{12}$	$(2.52 \pm 0.25) \times 10^{13}$	$(1.05 \pm 0.40) \times 10^{13}$
7	Beach (1994)	Hay Creek catchment	USA	Continental	125	AD 1851–1988	$1.53 \times 10^{13}$	$(3.33 \pm 0.33) \times 10^{12}$	$(2.40 \pm 0.24) \times 10^{12}$	$(2.89 \pm 0.70) \times 10^{12}$
8	Beach (1994)	Beaver Creek catchment	USA	Continental	144	AD 1851–1988	$1.97 \times 10^{13}$	$(7.89 \pm 0.79) \times 10^{12}$	$(6.21 \pm 0.63) \times 10^{12}$	$(7.04 \pm 0.75) \times 10^{12}$
9	van Hooff and Jungerius (1984)	Gultland catchment	Luxembourg	Temperate	38.8	2000 BC–AD 1984	$3.23 \times 10^{13}$	$(1.12 \pm 0.11) \times 10^{13}$	$(6.43 \pm 1.49) \times 10^{13}$	$(2.64 \pm 0.72) \times 10^{13}$
10	Trimble (1981)	Coon Creek catchment	USA	Continental	360	AD 1853–AD 1975	$6.16 \times 10^{13}$	$(1.08 \pm 0.11) \times 10^{13}$	$(5.79 \pm 0.58) \times 10^{13}$	$(8.21 \pm 1.21) \times 10^{12}$
11	O'Hara et al. (1993)	Patzcuaro Lake catchment	Mexico	Temperate	801	2000 BC–AD 2000	$1.17 \times 10^{14}$	$(4.11 \pm 0.96) \times 10^{13}$	$(4.58 \pm 0.86) \times 10^{14}$	$(2.25 \pm 0.78) \times 10^{14}$
12	Van Oost et al. (2012)	Dijle catchment	Belgium	Temperate	780	4000 BC–AD 2000	$7.11 \times 10^{14}$	$(3.87 \pm 0.53) \times 10^{13}$	$(2.48 \pm 0.43) \times 10^{15}$	$(7.78 \pm 3.70) \times 10^{14}$
13	Hoffmann et al. (2013)	Rhine River catchment	Central Europe	Temperate	130,000	5500 BC–AD 2000	$167 \times 10^{17}$	$(3.61 \pm 0.61) \times 10^{16}$	$(4.30 \pm 0.54) \times 10^{17}$	$(1.69 \pm 0.63) \times 10^{17}$
14	Saito et al. (2001)	Yellow River catchment	China	Temperate	752,443	AD 1–2000	$3.87 \times 10^{17}$	$(10.64 \pm 2.32) \times 10^{16}$	$(6.30 \pm 0.63) \times 10^{17}$	$(3.06 \pm 0.90) \times 10^{17}$

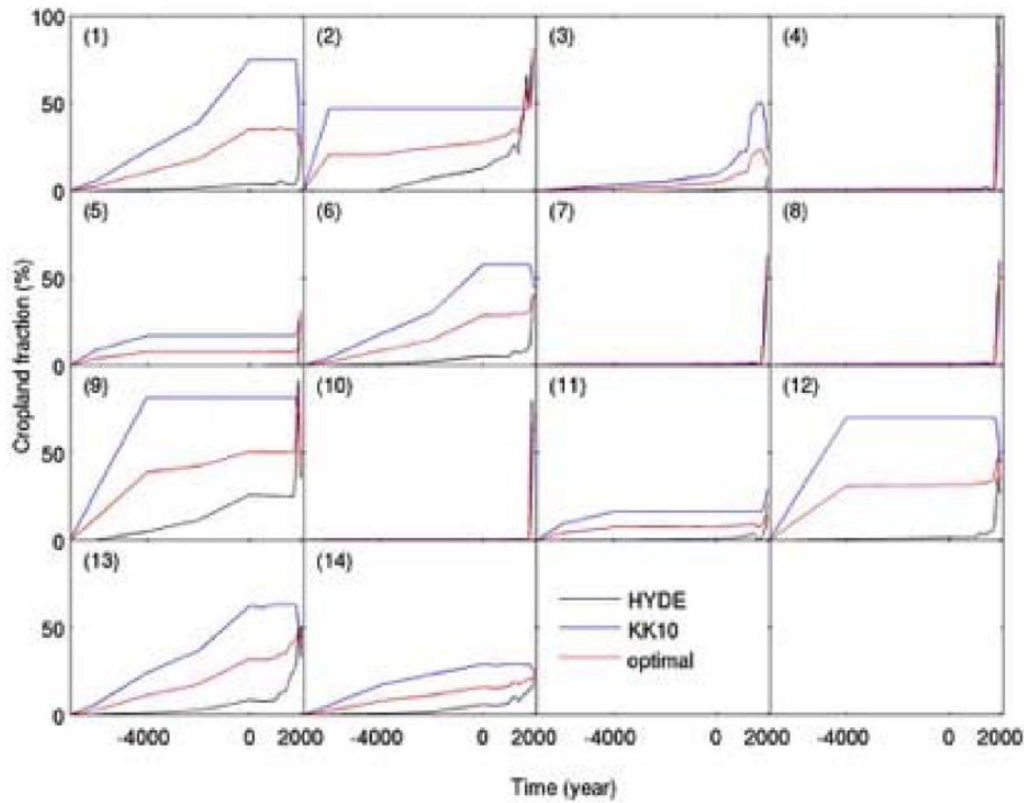


**Figure 2.** Temporal evolution of the fraction of cropland in the catchments studied. The numbers in parentheses denote the identification of the catchment, which is shown in Table 1.

$$E_0 = \alpha \times E \quad (2)$$

where  $E_0$  ( $\text{m yr}^{-1}$ ) is soil erosion at the beginning of agriculture,  $E$  ( $\text{m yr}^{-1}$ ) is the present-day erosion, and  $\alpha$  is a factor to scale the erosion. For each catchment, the total area of cropland is easy to obtain from the land-use history, while the eroding area is variable depending on the ratio of eroding area to depositional area. Thus, for a given amount of total erosion, it is easier to use the average erosion rate (per unit area) of the whole cropland catchment than that of the eroding area.

The erosion (per unit area of cropland) of a given period was then linearly related to the cropland area:

$$E(t) = \frac{E_0}{A_0} \times A(t) \quad (3)$$

where  $E(t)$  ( $\text{m yr}^{-1}$ ) is the average erosion in period  $t$ ,  $A_0$  ( $\text{m}^2$ ) is the cropland area at the beginning stage of agriculture, and  $A(t)$  ( $\text{m}^2$ ) is the cropland area of period  $t$ .

The amount of soil that is cumulatively eroded for a given catchment was calculated as follows:

$$S_{e,t} = \sum_{t=1}^n E(t) \times A \times B \times T(t) \quad (4)$$

where  $S_{e,t}$  (kg) is the cumulatively eroded sediments until period  $t$ ,  $A$  is the area of the catchment ( $\text{m}^2$ ),  $B$  ( $\text{kg m}^{-3}$ ) is the soil bulk density,  $T(t)$  (yr) is the length of period  $t$ , and  $n$  is the number of period.

#### Land-use scenarios

Given that land cover change is the main driver of our model, we used two frequently used but different ALCC scenarios, that is, HYDE (Klein Goldewijk et al., 2010, 2011) and KK10

(Kaplan et al., 2011) as the basis for our study. However, these two ALCC scenarios strongly differ in their estimates of per capita land use at low population densities. The conversion of non-cropland to cropland occurs at a much higher rate during the early phases for the KK10 scenario. This difference in cropland area evolution results in substantial differences in our simulations of cumulative agricultural soil erosion between these two base scenarios.

#### Model calibration and validation at the catchment scale

Simulation of cumulative erosion requires information on erosion per unit area of cropland and the temporal evolution of cropland area. The present-day average erosion of the 14 catchments where measured data are available was extracted from the map presented by Van Oost et al. (2007) (Table 1). To account for the uncertainty associated with the estimation of the erosion, we introduced a scaling factor:

$$E_{scaled} = \beta \times E_{average} \quad (5)$$

where  $E_{scaled}$  is the scaled erosion ( $\text{m yr}^{-1}$ ),  $\beta$  is the parameter to scale the erosion, and  $E_{average}$  ( $\text{m yr}^{-1}$ ) is the average erosion of a given catchment.

The temporal evolution of cropland area for the 14 catchments was then extracted from the HYDE and KK10 land-use scenarios (Figure 2). The cumulative erosion mobilized in a catchment because of agricultural erosion by water is related to its land-use history as it integrates changes in cropland area and average erosion over time. We performed two tests: (1) we assumed that the reconstruction of the existing two land-use scenarios was correct, and estimated the erosion required to obtain the observed long-term cumulative erosion; (2) we assumed that the estimation of erosion was robust, and optimized the land-use scenarios to obtain

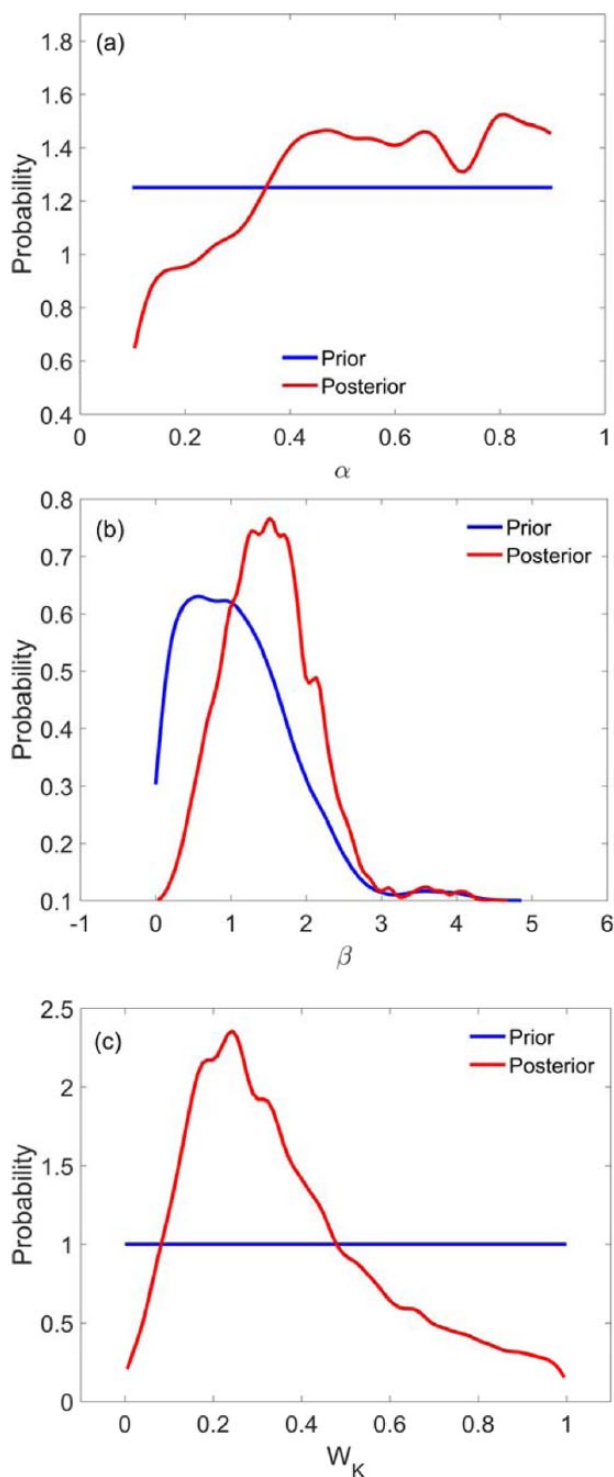


**Figure 3.** Prior and posterior distribution of the model parameters in the GLUE processing. (a)  $\alpha$  is the ratio of the erosion rate at the beginning of agriculture to that of the current day (Eq.2). (b)  $\beta$  is a scaling factor of the erosion rate to address the spatial uncertainties of erosion rate (Eq. 5). (c)  $W_k$  is a weighting factor representing the relative contribution of KK10 land use scenario in the integrated land use scenario (Eq. 6).

the observations. In the latter test, we generated new land-use scenarios by integrating HYDE and KK10 land-use scenarios:

$$A(t) = W_K \times A_K(t) + (1 - W_K) \times A_H(t) \quad (6)$$

where  $A(t)$  ( $m^2$ ) is the cropland area at time  $t$  (yr) in the combined land-use scenario,  $A_H(t)$  ( $m^2$ ) and  $A_K(t)$  ( $m^2$ ) are the cropland area at time  $t$  (yr) in the HYDE and KK10 land-use scenarios, respectively, and  $W_K$  is a weighting factor that ranges between 0 and 1.

To address the uncertainties associated with these variables, we explored an entire range of possible model parameter sets by modeling cumulative anthropogenic erosion as a series of 10,000 Monte Carlo series. In each Monte Carlo scenario,  $\alpha$  and  $W_k$  were randomly selected assuming a uniform distribution within a realistic range (Figure 3). To account for the spatial uncertainties of the model prediction,  $\beta$  was selected from a distribution based on the variability of the model prediction of the NRI data. We standardized the simulated erosion of all the catchments in NRI data by the average of the erosion, and this standardized erosion was fitted into kernel density probability (kdf). In each Monte Carlo scenario,  $\beta$  was randomly selected from the distribution derived from kdf. The probability distributions of  $\alpha$ ,  $\beta$ , and  $W_k$  were estimated using generalized likelihood uncertainty estimation (GLUE; Beven and Binley, 1992) by confronting the simulated cumulative anthropogenic erosion with measurements of the 14 catchments (Table 1). The root mean square (RMS) of the residuals of a simulation scenario was assessed using the following equation:

$$RMS(i) = \sum_{k=1}^n \sqrt{\frac{(\log Sim_{k(i)} - \log Obs_k)^2}{n}} \quad (7)$$

where  $RMS(i)$  is the root mean square of the residuals of scenario  $i$ ,  $Sim_{k(i)}$  (kg) and  $Obs_k$  (kg) are the simulated and observed anthropogenic sediments in scenarios  $i$  of the catchment  $k$ , respectively, and  $n$  is the number of catchments. Given that the anthropogenic erosion of these catchments spans over a magnitude of seven orders, the logarithms of observations and simulations were used to avoid observations having different weights in the calibration. The reciprocal of the RMS of the residuals was used as the likelihood of this scenario. The derived likelihood of each scenario was then used to quantify the probability distributions of the model output at the catchment or global scales using the methodology described by Beven and Binley (1992).

To validate our simulation of the cumulative erosion at the catchment scale, we used a jackknife (leave one out) resampling technology, that is, we selected 13 catchments and estimated the weights of the parameter sets with the observed cumulative erosion using GLUE, and predicted the cumulative anthropogenic erosion of the remaining one catchment. In a final series of simulations, we therefore used all 14 catchments to constrain the ALCC weighting factor ( $W_k$ ), using the same probabilistic approach as described above. This distribution was used in consecutive simulations of cumulative anthropogenic erosion across the globe.

The absolute difference of the logarithms (ADL) was introduced to assess the goodness of prediction for a given catchment:

$$ADL(i) = |\log Sim_{(i)} - \log Obs| \quad (8)$$

where  $ADL(i)$  is the absolute difference of the logarithms of the observation and simulation under a given land-use scenario for a given catchment in scenario  $i$ .  $Sim(i)$  is the simulation in scenario  $i$  of a given catchment and  $Obs$  is the observation of a given catchment.

The simulations under different land-use scenarios were compared using the Akaike information criterion (AIC) (Akaike, 1998). We used a definition of AIC without an explicit quantification of measurement error (Pelletier, 2012):

$$AIC = n \times 1n \left( \frac{RSS}{n} \right) + 2k + \frac{2k(k+1)}{n-k-1} \quad (9)$$

where  $RSS$  is the residual sum of squares (equal to the sum of the differences between the logarithms of the predicted and observed

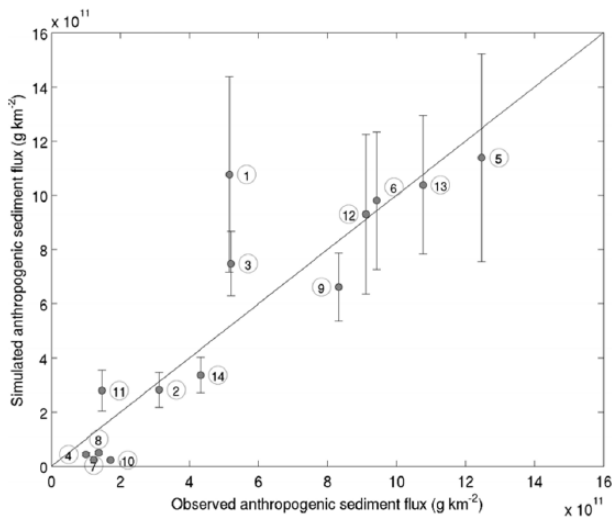


**Figure 4.** Simulated anthropogenic sediment fluxes using the parameters constrained with the observed data of all 14 catchments. The error bars show the interquartile range (25–75%) of the distribution (obtained from Monte Carlo scenarios) associated with each simulation. The numbers in circles denote the identification of the catchment, which is shown in Table 1.

data),  $n$  is the number of data points, and  $k$  is the number of free parameters in the model.

To identify the controlling factors on the cumulative anthropogenic erosion, we performed two tests by using only one of the two factors (land-use change and soil erosion) to optimize the model, that is: (1) we used the site-specific erosion and a common land-use scenario (i.e. a cumulative time-weighted cropland area) of the 14 catchments and (2) we used the site-specific land-use change and a common soil erosion for all the 14 catchments. The models were optimized based on observations, and their performance was evaluated using *AIC*.

#### Model implementation across the globe

The model was implemented across the globe in a Monte Carlo approach. In all, 1000 Monte Carlo simulations were performed in total. In each Monte Carlo simulation, the values of  $\alpha$ ,  $\beta$ , and  $W_k$  were randomly generated from their posterior distributions after the GLUE processing. For each grid in the simulation, the best prediction of the erosion was derived from the median value of the Monte Carlo simulation. The relative prediction uncertainties were calculated as:

$$E_u = \frac{(Q_{75} - Q_{25})}{Q_{50}} \quad (10)$$

where  $E_u$  (%) is the relative uncertainties in the prediction of erosion, and  $Q_{75}$ ,  $Q_{50}$ , and  $Q_{25}$  are the 75th, 50th, and 25th percentiles, respectively, of the predictions in the Monte Carlo simulation.

## Results

If HYDE land-use scenario is assumed to represent the historical land-use change, precise estimations of the measured long-term anthropogenic erosion require erosion that is  $5.08 \pm 1.54$  times of the estimated soil erosion by Van Oost et al. (2007). In contrast, if KK10 land-use scenario is assumed to represent the historical land-use change, precise estimations of the field measured long-term anthropogenic erosion require erosion that is  $0.61 \pm 0.24$  times of the estimated soil erosion by Van Oost et al. (2007). Given that erosion estimated by Van Oost et al. (2007) was well constrained by NRI measurements, the large deviations of the erosion indicate that

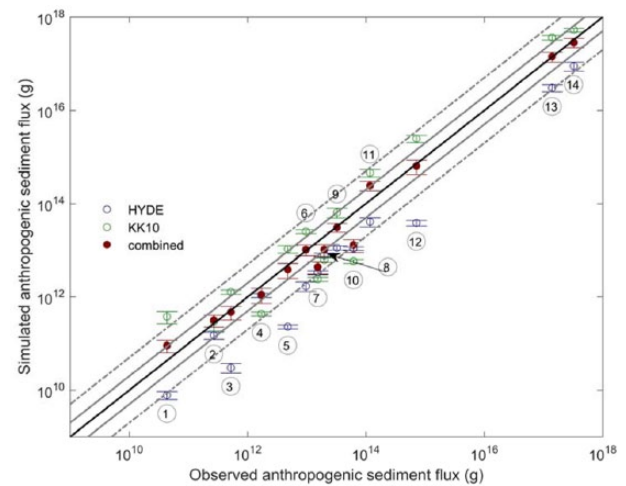


**Figure 5.** Model validation at the catchment scale using the observed anthropogenic sediment flux. The numbers in circles denote the identification of the catchment, which is shown in Table 1. HYDE and KK10 denote the predictions using the HYDE and KK10 land-use scenarios. The red circles denote the predictions using the land-use scenario combining both HYDE and KK10. The error bars indicate the range of 25% and 75% of all the Monte Carlo scenarios. The black solid line denotes the ratio of 1:1. The gray solid lines denote the ratio of 1:2 and 2:1. The gray dashed lines denote the ratio of 1:5 and 5:1.

these two land-use scenarios are not consistent with our current understanding of the variability in erosion across the globe and therefore may not well represent past land-use change. We then used an alternative approach where we assumed that the soil erosion estimates are robust by optimizing the land-use scenarios. Optimization using all the 14 catchments shows that the model simulations using the combined land-use scenario can capture well the order of magnitude of the observations with a relative error of ca. 0.43 (Figure 4). The GLUE approach can change the prior uniform distribution of the parameters within the parameter range (Figure 3). The values of 25th, 50th, and 75th quantiles of the prior distribution of  $\beta$  are 0.52, 1.00, and 1.53, while that of the posterior distribution are 1.09, 1.48, and 1.88. The posterior distribution of  $\alpha$  is skewed to the left with the values of 25th, 50th, and 75th quantiles being 0.39, 0.59, 0.60, respectively, while that of  $W_k$  is skewed to the right with the values of 25th, 50th, and 75th quantiles being 0.20, 0.32, and 0.50.

Using the validated erosion by Van Oost et al. (2007), simulations under the HYDE land-use scenario systematically underestimate the cumulative anthropogenic erosion for all the catchments (Table 1, Figure 5). In contrast, simulations under the KK10 scenario make overestimations except at the four catchments in the US. Validation using jackknife resampling technology show that results under the combined scenarios are between simulations under one of the two scenarios, and fit the observed results better than using only one scenario. The ADL under the optimized land-use scenario is  $0.19 \pm 0.21$ , which is significantly smaller than under HYDE ( $0.69 \pm 0.36$ ) and KK10 ( $0.51 \pm 0.27$ ) land-use scenarios ( $p < 0.05$ , Mann–Whitney U-test, Figure 6). Similar to the ADL, the AIC under the optimized land-use scenario is 733.9, which is smaller than that under HYDE (762.4) and KK10 (789.6) scenarios. Also, the AIC value of this model is smaller than that of the models only considering erosion (747.2) or land-use change (744.6). This suggests that our combined land-use scenario is the best predictor.

If it is accepted that the combined land-use scenario presented in this study describes well past land cover change, it can be used to apply the erosion model across Earth for the agricultural period. The cumulative anthropogenic erosion until the present-day is estimated to be  $27,187 \pm 9030$  Pg under the combined land-use

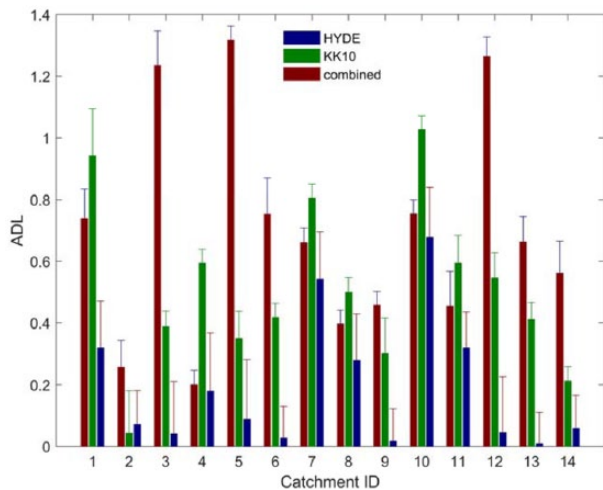


**Figure 6.** The absolute difference of the logarithms (ADL, Eq. 8) between the simulations and observations. Information on the catchment ID is shown in Table 1.

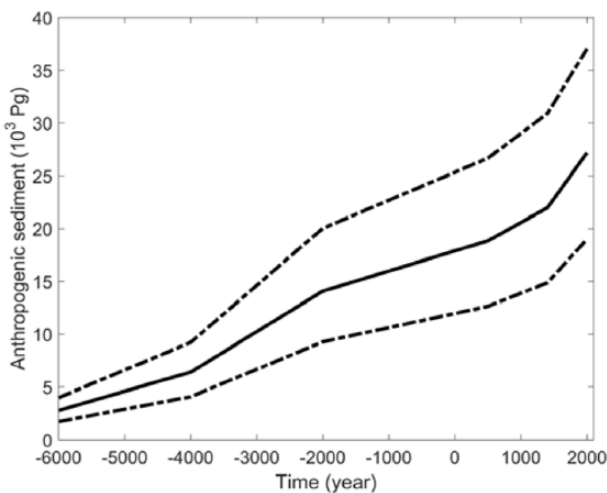


**Figure 7.** Temporal evolution of the cumulative global anthropogenic erosion under the combined land-use scenarios. The solid line represents the median model simulation while the dotted lines represent the 25th and 75th percentiles.

change scenario (Figure 7). The average cumulative soil erosion of the cropland is estimated to be  $1829 \pm 613 \text{ kg m}^{-2}$ , which equals loss of soil depth of  $1.34 \pm 0.45 \text{ m}$  (Figure 8). Regions of earlier civilization have larger cumulative anthropogenic erosion (Figure 9). South Asia, Southeast Asia, East Asia, Africa, South America, Central America, and Europe have high cumulative erosion (exceeding  $2000 \text{ Pg}$ , Table 2). South Asia, Southeast Asia, and Central America have the highest area-averaged anthropogenic erosion of ca.  $1.2 \text{ Tg km}^{-2}$  (Table 2, Figure 10). This results in an average soil truncation of ca.  $0.9 \text{ m}$ . Europe and East Asia also have relatively high anthropogenic erosion of ca.  $0.35 \text{ Tg km}^{-2}$ . This results in an average soil truncation of ca.  $0.26 \text{ m}$ . The prediction uncertainty ranges between 36% and 100% with a mean of 66% (Figure 11). The mass-weighted sediment age generally increases with time, but experiences a sharp decrease in the last two centuries in regions where large areas have been converted to agricultural use.

## Discussion

Correct estimation of the observed long-term anthropogenic erosion under HYDE and KK10 land-use scenarios requires  $5.08 \pm$

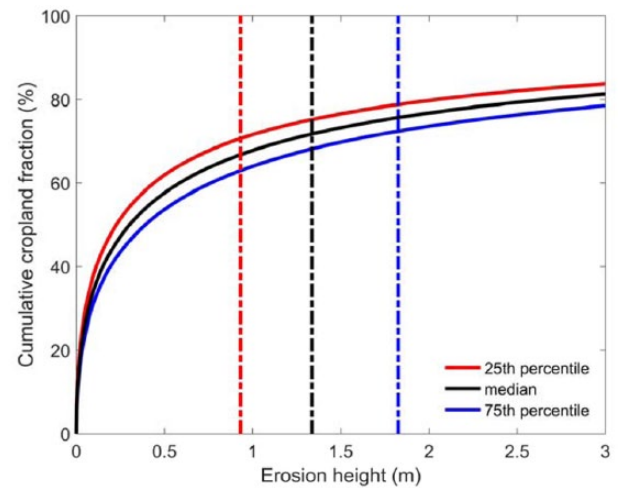


**Figure 8.** Cumulative distribution of erosion height on the cropland under the combined land-use scenarios. The dotted lines indicate the area-weighted average erosion height.

$1.54$  and  $0.61 \pm 0.24$  times of the earlier published average soil erosion. Given that the global soil erosion was validated using observations from the US (NRCS, 2007) and Europe (Cerdan et al., 2010), it suggests that a more likely cropland expansion scenario should be located between the HYDE and KK10 land-use scenarios. This implies that, if it is accepted that the sedimentary record provides a solid basis to constrain past land cover change, the assumed relationship between population and anthropogenic land use used in HYDE underestimates the per capita land use while that in KK10 overestimates per capita land use. By linearly combining the two land-use scenarios, we attempted to give a first spatially explicit estimation of the cumulative anthropogenic erosion. Our simulation resulted in a global cumulative agricultural erosion of  $27,187 \pm 9030 \text{ Pg}$  for the period of agriculture. This is larger, but in the same order of magnitude than the earlier assessment that humans have displaced approximately  $20,000 \text{ Pg}$  of sediments through cropland erosion over the history of civilization (Wilkinson and McElroy, 2007). Nevertheless, we argue that our approach provides a more robust estimate of cumulative agricultural erosion because our estimates were not simply extrapolated from a single population estimate (as was done in Wilkinson and McElroy (2007)), but were calculated using a spatially explicit approach in which field observations and two contrasting ALCC scenarios were used to constrain and evaluate the model. The relatively prediction uncertainty of our approach on the cumulative anthropogenic erosion is below 100% (Figure 11), which is acceptable given the spatial scale and the temporal scale considered in this study. Also, the regions of low uncertainty are Europe, China, India, and the US where the cumulative anthropogenic erosion is high. The coincidence of these two spatial patterns could be because of the fact that differences between HYDE and KK10 land-use scenarios are smaller in the regions of higher population density. This guarantees a good estimation of the total global cumulative anthropogenic erosion.

The RUSLE model is usually developed and calibrated using point measurements of erosion. This hampers its application at larger scales, because it will result in a scale issue if the model is further applied at catchment scale because of the nonlinear relationship between erosion measurements at different scales. Our approach is free of this scale issue because we used area estimates of soil loss provided by the NRI assessment (US National resource inventory) to calibrate our erosion model. The NRI data report statistical survey of soil erosion of the US. They are incorporated into estimation procedures in such a way that the NRI database is representative of the spatial distribution of soil erosion and hence

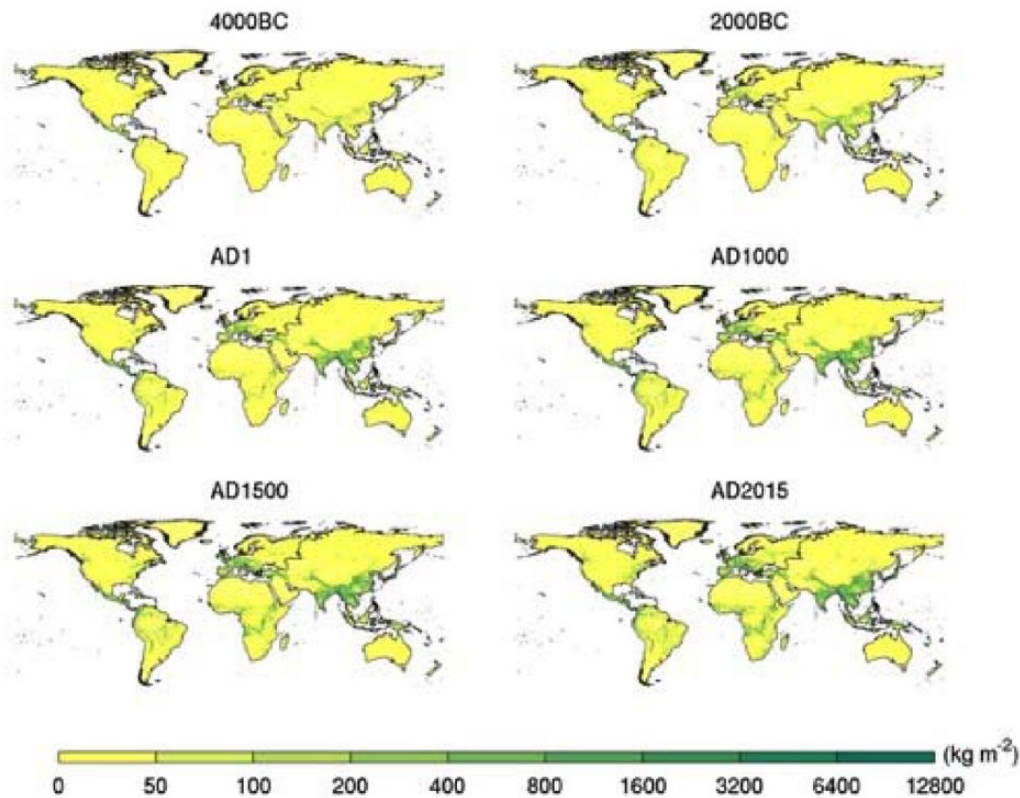


**Figure 9.** Maps of cumulative anthropogenic sediment fluxes under the optimal land-use scenario from the onset of agriculture to the years of 4000 BC, 2000 BC and AD 1, 1000, 1500, and 2015.

**Table 2.** Cumulative erosion of different regions under the combined land-use scenario.

Regions	Area (km <sup>2</sup> )	Cumulative erosion (10 <sup>3</sup> Pg)	Area-average cumulative erosion (Tg km <sup>-2</sup> )
Africa	$2.9 \times 10^7$	$3.34 \pm 1.16$	$0.12 \pm 0.040$
Oceania	$7.8 \times 10^6$	$0.33 \pm 0.12$	$0.043 \pm 0.016$
Southeast Asia	$3.6 \times 10^6$	$4.29 \pm 1.53$	$1.19 \pm 0.42$
South Asia	$4.3 \times 10^6$	$4.73 \pm 1.69$	$1.10 \pm 0.39$
West Asia	$5.8 \times 10^6$	$0.86 \pm 0.25$	$0.15 \pm 0.042$
Central Asia	$4.4 \times 10^6$	$0.35 \pm 0.12$	$0.080 \pm 0.028$
East Asia	$9.5 \times 10^6$	$3.87 \pm 1.27$	$0.43 \pm 0.14$
North Asia	$1.3 \times 10^7$	$0.094 \pm 0.030$	$0.0073 \pm 0.0023$
Europe	$8.5 \times 10^6$	$2.49 \pm 0.75$	$0.29 \pm 0.089$
South America	$1.7 \times 10^7$	$3.11 \pm 0.87$	$0.18 \pm 0.051$
Central America	$2.3 \times 10^6$	$2.78 \pm 0.97$	$1.21 \pm 0.42$
North America	$1.7 \times 10^7$	$0.96 \pm 0.30$	$0.056 \pm 0.018$
Total	$1.2 \times 10^8$	$27.19 \pm 9.03$	$0.22 \pm 0.075$

meaningful areal estimates can be made (Nusser et al., 1999). Validation of our erosion model using basin-average soil losses (NRI data) shows that slope, rainfall erodibility, and crop type can explain the 57% of the observation variability (Doetterl et al., 2012). Given that the model focuses on the global scale, it only takes into account a limited number of factors that are dominant in controlling erosion, while other factors that drive small-scale variations are not captured in the model. For instance, erosion may vary with crop type with fields under plants such as potatoes and sugar beets more erodible. However, crop type varies between small regions or cropland parcels, which is difficult to represent in our global-scale model. Land management measures such as traditional tillage and conservation tillage also have an important effect on erosion, but data on the land management at the global scale are not easy to obtain. Factors such as soil erodibility and

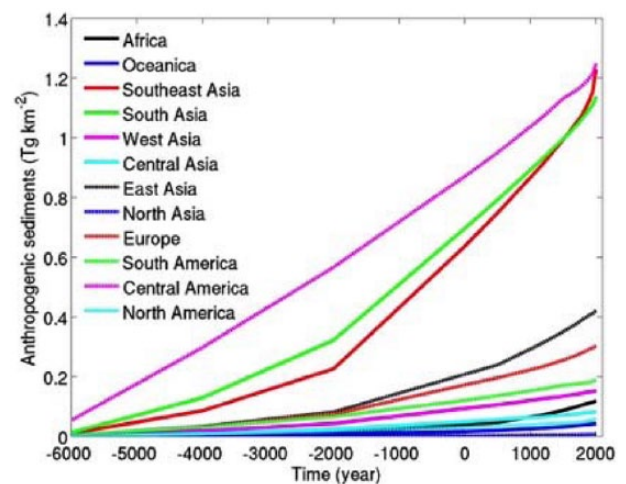


**Figure 10.** Temporal evolution of the anthropogenic sediment fluxes in different regions under the optimal land-use scenario.

slope length may not show significant variability between catchments, and therefore they are not included in the model applied at larger spatial scales (Doetterl et al., 2012; Van Oost et al., 2007).

The cumulative anthropogenic erosion in a catchment is related to its land-use history as it integrates changes in cropland area and average erosion over time. Thus, our assessment on the land-use scenarios using data of long-term anthropogenic erosion relies on reliable information on the cropland soil erosion. In this study, the present-day average erosion estimated by Van Oost et al. (2007) was validated using the observed erosion in the US (NRCS, 2007). However, estimation of the cumulative erosion also requires the erosion in the past. We derived the erosion in the past by taking into account the fact that flatter areas have a larger likelihood to be converted as cropland first, and therefore the average slope of the

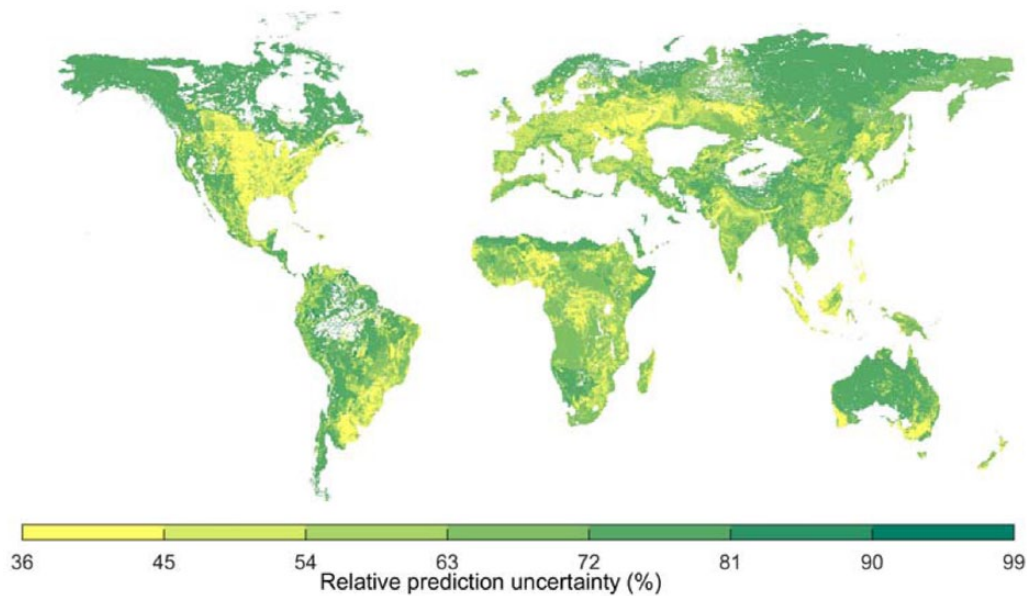


**Figure 11.** The relative prediction uncertainty (%),  $(Q_{75} - Q_{25})/Q_{50}$  of the cumulative anthropogenic erosion.

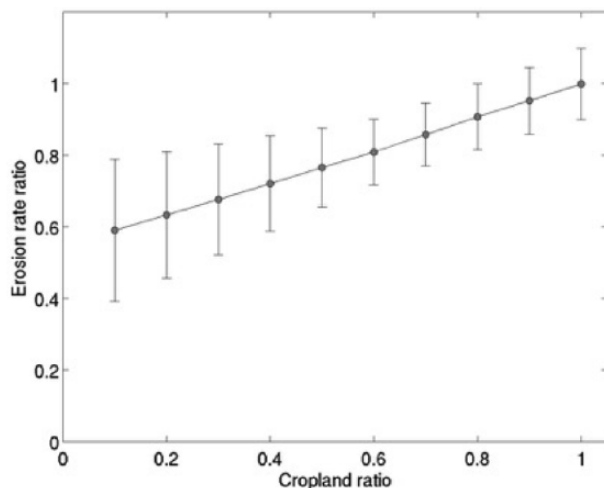


**Figure 12.** The effect of cropland area on the erosion rate (per unit area of cropland). Erosion rate ratio denotes the ratio of erosion rate at a given time to the current-day erosion rate and is calculated using Eq. 3. Cropland ratio denotes the ratio of cropland area at a given time to the cropland area of current-day. The error bars show the interquartile range (25–75%) of the distribution (obtained from Monte Carlo scenarios) associated with each simulation.

cropland increases with the increasing cropland area (Van Rompaey et al., 2001). This results in the simulation that the erosion (per unit area of cropland) temporally varies in the range of 55–100% of the current-day erosion (Figure 12), which, however, is not validated. Other factors that affect the temporal variation of the soil erosion such as land management are not considered in our assessment. Sediment fluxes in the Chinese rivers were observed to decrease in the past decades, which was partly attributed to the soil and water conservation (Chu et al., 2009; Wang et al., 2016). Furthermore, the erosion in the cropland of the US has decreased in the past decades because of improved land management (NRCS, 2007). This may be one of the reasons why our estimation in both HYDE and KK10 scenarios underestimated the anthropogenic erosion in the four catchments in the US (Figure 5). Thus, the cumulative anthropogenic erosion in the US may be underestimated in our study. Despite the drawbacks discussed above, this

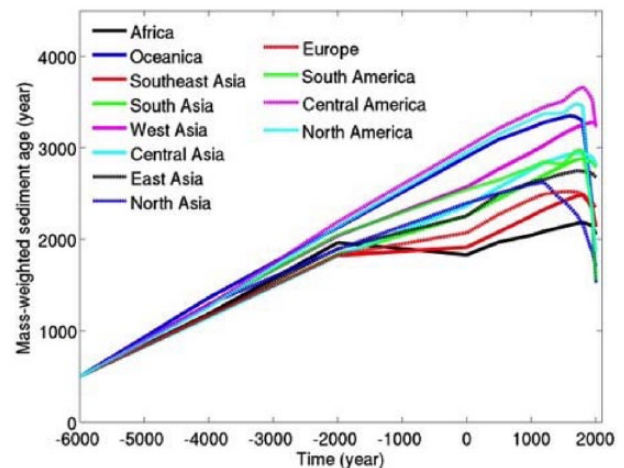


**Figure 13.** Temporal evolution of mass-weighted age of the anthropogenic sediments under the optimal land-use scenario for different regions for the area where the fraction of current-day cropland is higher than 50%.

study gives a robust spatial-explicit estimation of the cumulative anthropogenic erosion that is consistent with previous estimation (Wilkinson and McElroy, 2007). This can be attributed to the following two facts: (1) the observation data of long-term anthropogenic erosion span over various conditions with a good represent of the world, that is, the 14 catchments are located on different continents with different climate and agricultural histories and (2) our approach has captured the most important factors, such as land use, topography, and precipitation, that control the long-term anthropogenic erosion at the global scale.

We also emphasize that the two existing land-use scenarios were simply linearly integrated using a weighting factor, and that our approach is therefore not based on known processes or relationship related to anthropogenic land-use expansion. Furthermore, this weighting factor was constrained using the total cumulative anthropogenic erosion with uncertainties on possible factors controlling the temporal variation of the erosion on the cropland. Thus, the pattern of the temporal variation of the ALCC and the consequent anthropogenic erosion require further validation.

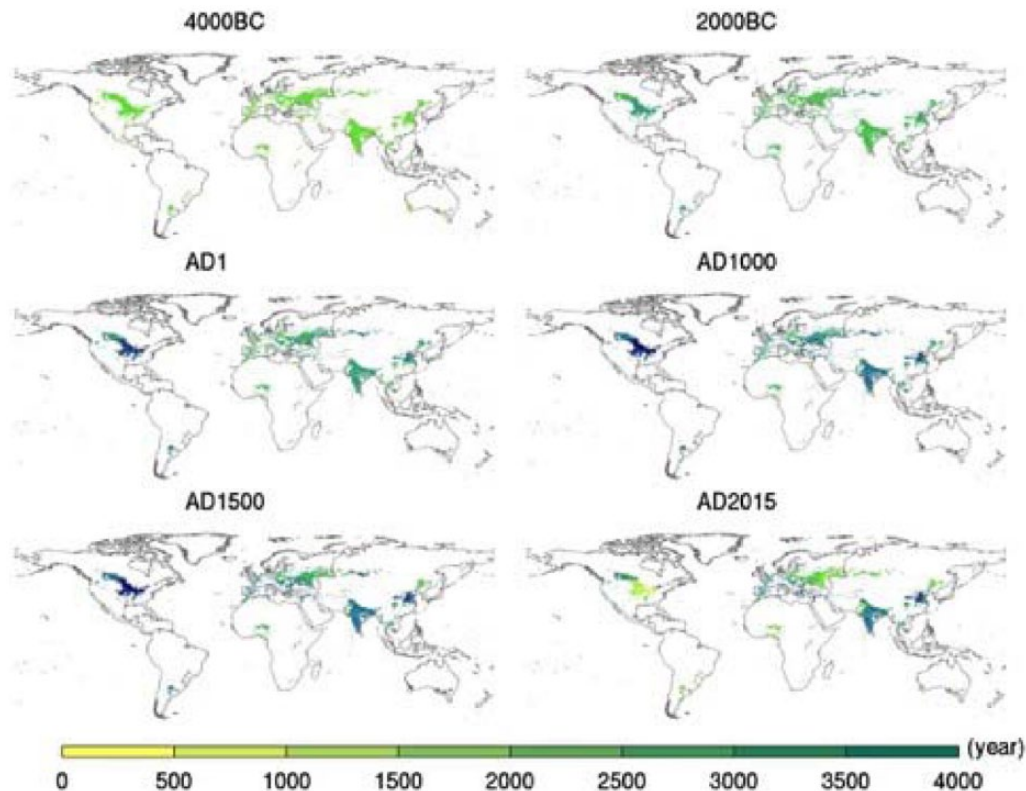


**Figure 14.** Maps of mass-weighted sediment age under the optimal land-use scenario for the timeslices 4000 BC, 2000 BC, and AD 1, 1000, 1500, and 2015 for the area where the fraction of current-day cropland is higher than 50%.

The redistribution of the eroded sediments within the catchment as well as their export from the catchment can have an important effect on the relevant geomorphic units. At the eroding areas, the cumulative soil truncation can be of the order of meters (Figure 8). This soil truncation may enhance the in situ soil chemical weathering rate and hence the soil production rate (Heimsath et al., 1997; Yoo et al., 2009). However, data drawn from a global compilation of studies show that erosion from conventionally plowed agricultural fields is on average 1–2 orders of magnitude of soil production rates (Montgomery, 2007). This shows the importance to reduce soil erosion for the purpose of agricultural sustainability. Compilation by Webb and Rosenzweig (1993) shows that global soil thickness exhibits a crude log-normal distribution with a mean of ca. 1.3 m, which is equivalent to the average cumulative erosion soil height of the cropland in our estimation (ca. 1.34 m). This implies that the remaining soil reservoir in the cropland may last for millennia under the condition of current-day soil erosion on cropland. This is consistent with the analysis by Wilkinson and McElroy (2007), who showed that under the erosion of  $0.6 \text{ mm yr}^{-1}$ , the cropland soil area would reduce by ca. 0.04% per year, and it would take several thousand years to lose the total soil reservoir. The reduction of soil depth can decrease the supply of water, nutrients and rooting space and hence decrease the net primary production (NPP) of cropland (Bakker et al., 2007; Lal, 2003). At the same time, C depleted subsoil material is brought to the surface layers where it can be mixed with fresh photosynthetically derived C inputs. This additional C uptake may (at least partially) replace the laterally lost SOC because of erosion (Berhe et al., 2008; Harden et al., 1999). Field studies show that a large fraction of the mobilized soils by agricultural erosion are deposited close to sites of erosion, that is, the footslope of the upland (Beach, 1994; Notebaert et al., 2009; Rommens et al., 2005). Soil truncation at the shoulder slope and deposition at the footslope result in reduction of the slope gradient for the cropland and hence continuously alter the topography

(Peeters et al., 2006; Rommens et al., 2007). Previous studies show that SOC associated with the sediments buried in colluvial soils exponentially decreases with time and reaches an equilibrium C burial efficiency of ca. 20% after centuries (Van Oost et al., 2012; Wang et al., 2014). The result that the average age of the anthropogenic sediments ranges from centuries to millennia (Figure 13) indicates that most of the SOC originally associated with the sediments at the time of deposition has been mineralized. Regions such as Oceania, Africa, and North America that experience an expansion of cropland in recent periods have relatively low average sediment ages (Figures 13 and 14) because of the production of relatively young sediments. The sediments in these regions should therefore contain a higher fraction of original SOC because of the young age.

The accelerated erosion generally results in an increase of alluvial sedimentation in floodplains (Hoffmann et al., 2007; Verstraeten et al., 2009). Field studies show that a large amount of SOC is stored in these alluvial sediments (Hoffmann et al., 2009, 2013; Omengo et al., 2016). Our simulation suggests that the present-day sediment production caused by accelerated erosion from cropland is ca.  $11.7 \text{ Pg yr}^{-1}$ . The range of the sediment delivery ratios of the hillslope (i.e. the ratio of eroded sediments that are yielded to those reaching the river system) and river (i.e. the ratio of sediments entering the river system to those reaching the ocean) typically range from 30% to 50% (Notebaert et al., 2009; Phillips, 1991; Rommens et al., 2005, 2006; Verstraeten and Prosser, 2008). This implies that ca.  $1.1\text{--}2.9 \text{ Pg yr}^{-1}$  of human-induced sediments are exported to the ocean. This export rate is consistent with the estimation that humans have increased global sediment transport by rivers through soil erosion by  $2.3 \pm 0.6 \text{ Pg yr}^{-1}$ , based on a river-by-river analysis (Syvitski et al., 2005). Cumulatively, the accelerated erosion has resulted in ca. 2439–6776 Pg sediments exported to the ocean. The magnitude and temporal variability of soil and C erosion estimated in our study imply that soil erosion-induced C fluxes should not be neglected

in the global C cycling. Our study shows that soil characteristics could change over time because of erosion. However, Earth System Models (ESM) assume that the soil has remained static over time. These processes should be considered in ESM as it may result in a considerable difference to climate projections.

## Conclusion

Quantification of anthropogenic sediments is important to understand the role of human activities in ecosystem evolution. Our study shows that empirical data of long-term anthropogenic erosion at the catchment scale can be used to validate existing land-use scenarios in combination with a spatially distributed soil erosion model. Simulations show that HYDE land-use scenario underestimates the anthropogenic erosion while the KK10 scenario results in an overestimation. Validation at the catchment scale shows that scenarios integrating both existing land-use scenarios can result in a robust estimation of anthropogenic erosion. Application of the model under the optimal land-use scenario shows that conversion from natural vegetation to cropland has caused a global cumulative agricultural erosion of  $27,187 \pm 9030$  Pg for the period of agriculture. This results in an average cumulative sediment mobilization of  $1829 \pm 613$  kg m<sup>-2</sup> for croplands, which corresponds to an average soil truncation of ca.  $1.34 \pm 0.45$  m. Regions of early civilization and high cropland fractions such as South Asia, Southeast Asia, and Central America have experienced higher area-averaged anthropogenic erosion than other regions. More information on the fate of carbon and other key elements associated with the redistributed sediments because of anthropogenic erosion is needed to assess the consequent impacts of anthropogenic erosion on the ecosystem. Soil erosion should also be included in ESM given that it may change the characteristics of soils.

## Funding

This study was supported by BELSPO (IUAP program, contract: P7-24) and the Natural Science Foundation of China (Nos 41871014, 41771216, 41501450).

## References

- Akaike H (1998) A new look at the statistical model identification. In: Parzen E, Tanabe K and Kitagawa G (eds) *Selected Papers of Hirotugu Akaike*. New York: Springer, pp. 215–222.
- Anselmetti FS, Hodell DA, Ariztegui D et al. (2007) Quantification of soil erosion rates related to ancient Maya deforestation. *Geology* 35: 915–918.
- Bakker M, Govers G, Jones R et al. (2007) The effect of soil erosion on Europe's crop yields. *Ecosystems* 10: 1209–1219.
- Beach T (1994) The fate of eroded soil: Sediment sinks and sediment budgets of agrarian landscapes in Southern Minnesota, 1851–1988. *Annals of the Association of American Geographers* 84: 5–28.
- Berhe AA, Harden JW, Torn MS et al. (2008) Linking soil organic matter dynamics and erosion-induced terrestrial carbon sequestration at different landform positions. *Journal of Geophysical Research: Biogeosciences* 113: G04039.
- Beven K and Binley A (1992) The future of distributed models: Model calibration and uncertainty prediction. *Hydrological Processes* 6: 279–298.
- Cerdan O, Govers G, Le Bissonnais Y et al. (2010) Rates and spatial variations of soil erosion in Europe: A study based on erosion plot data. *Geomorphology* 122: 167–177.
- Chappell A, Baldock J and Sanderman J (2016) The global significance of omitting soil erosion from soil organic carbon cycling schemes. *Nature Climate Change* 6: 187–191.
- Chu ZX, Zhai SK, Lu XX et al. (2009) A quantitative assessment of human impacts on decrease in sediment flux from major Chinese rivers entering the western Pacific Ocean. *Geophysical Research Letters* 36: L19603.
- Ciampalini R, Billi P, Ferrari G et al. (2012) Soil erosion induced by land use changes as determined by plough marks and field evidence in the Aksum area (Ethiopia). *Agriculture, Ecosystems & Environment* 146: 197–208.
- de Vente J, Poesen J, Arabkhedri M et al. (2007) The sediment delivery problem revisited. *Progress in Physical Geography* 31: 155–178.
- Dearing JA, Håkansson H, Liedberg-Jönsson B et al. (1987) Lake sediments used to quantify the erosional response to land use change in southern Sweden. *Oikos* 50: 60–78.
- Doetterl S, Van Oost K and Six J (2012) Towards constraining the magnitude of global agricultural sediment and soil organic carbon fluxes. *Earth Surface Processes and Landforms* 37: 642–655.
- Enters D, Dörfler W and Zolitschka B (2008) Historical soil erosion and land-use change during the last two millennia recorded in lake sediments of Frickenhauser See, northern Bavaria, central Germany. *The Holocene* 18: 243–254.
- Fuchs M, Will M, Kunert E et al. (2011) The temporal and spatial quantification of Holocene sediment dynamics in a meso-scale catchment in northern Bavaria, Germany. *The Holocene* 21: 1093–1104.
- Harden JW, Sharpe JM, Parton WJ et al. (1999) Dynamic replacement and loss of soil carbon on eroding cropland. *Global Biogeochemical Cycles* 13: 885–901.
- Heimsath AM, Dietrich WE, Nishiizumi K et al. (1997) The soil production function and landscape equilibrium. *Nature* 388: 358–361.
- Heinz M, Graeber D, Zak D et al. (2015) Comparison of organic matter composition in agricultural versus forest affected headwaters with special emphasis on organic nitrogen. *Environmental Science & Technology* 49: 2081–2090.
- Hoffmann T (2015) Sediment residence time and connectivity in non-equilibrium and transient geomorphic systems. *Earth-Science Reviews* 150: 609–627.
- Hoffmann T, Glatzel S and Dikau R (2009) A carbon storage perspective on alluvial sediment storage in the Rhine catchment. *Geomorphology* 108: 127–137.
- Hoffmann T, Erkens G, Cohen KM et al. (2007) Holocene floodplain sediment storage and hillslope erosion within the Rhine catchment. *The Holocene* 17: 105–118.
- Hoffmann T, Schlummer M, Notebaert B et al. (2013) Carbon burial in soil sediments from Holocene agricultural erosion, Central Europe. *Global Biogeochemical Cycles* 27: 828–835.
- Hooke RL (2000) On the history of humans as geomorphic agents. *Geology* 28: 843–846.
- Houben P (2012) Sediment budget for five millennia of tillage in the Rockenberg catchment (Wetterau loess basin, Germany). *Quaternary Science Reviews* 52: 12–23.
- Houghton RA, House JI, Pongratz J et al. (2012) Carbon emissions from land use and land-cover change. *Biogeosciences* 9: 5125–5142.
- Kaplan JO, Krumhardt KM, Ellis EC et al. (2011) Holocene carbon emissions as a result of anthropogenic land cover change. *The Holocene* 21: 775–791.
- Klein Goldewijk K, Beusen A and Janssen P (2010) Long-term dynamic modeling of global population and built-up area in a spatially explicit way: HYDE 3.1. *The Holocene* 20: 565–573.
- Klein Goldewijk K, Beusen A, van Drecht G et al. (2011) The HYDE 3.1 spatially explicit database of human-induced global land-use change over the past 12,000 years. *Global Ecology and Biogeography* 20: 73–86.
- Lal R (2003) Soil erosion and the global carbon budget. *Environment International* 29: 437–450.
- Montgomery DR (2007) Soil erosion and agricultural sustainability. *Proceedings of the National Academy of Sciences of the United States of America* 104: 13268–13272.

- Muenich RL, Kalcic M and Scavia D (2016) Evaluating the impact of legacy P and agricultural conservation practices on nutrient loads from the Maumee River Watershed. *Environmental Science & Technology* 50: 8146–8154.
- Murphy GEP and Romanuk TN (2014) A meta-analysis of declines in local species richness from human disturbances. *Ecology and Evolution* 4: 91–103.
- Newbold T, Hudson LN, Hill SLL et al. (2015) Global effects of land use on local terrestrial biodiversity. *Nature* 520: 45–50.
- Notebaert B, Verstraeten G, Rommens T et al. (2009) Establishing a Holocene sediment budget for the river Dijle. *CATENA* 77: 150–163.
- NRCS (2007) *National Resources Inventory 2003 Annual NRI – Soil Erosion*. Summary report. Available at: <http://www.nrcs.usda.gov/technical/land/nri03/nri03eros-mrb.html>
- Nusser SM, Kienzler JM and Fuller WA (1999) Geostatistical Estimation Data for the 1997 National Resources Inventory. Working Paper. Available at: [https://www.nrcs.usda.gov/Internet/FSE\\_DOCUMENTS/stelprdb1042181.pdf](https://www.nrcs.usda.gov/Internet/FSE_DOCUMENTS/stelprdb1042181.pdf).
- O'Hara SL, Street-Perrott FA and Burt TP (1993) Accelerated soil erosion around a Mexican highland lake caused by prehispanic agriculture. *Nature* 362: 48–51.
- Oldfield F, Wake R, Boyle J et al. (2003) The late-Holocene history of Gormire Lake (NE England) and its catchment: A multiproxy reconstruction of past human impact. *The Holocene* 13: 677–690.
- Omengo FO, Geeraert N, Bouillon S et al. (2016) Deposition and fate of organic carbon in floodplains along a tropical semiarid lowland river (Tana River, Kenya). *Journal of Geophysical Research: Biogeosciences* 121: 1131–1143.
- Peeters I, Rommens T, Verstraeten G et al. (2006) Reconstructing ancient topography through erosion modelling. *Geomorphology* 78: 250–264.
- Pelletier JD (2012) A spatially distributed model for the long-term suspended sediment discharge and delivery ratio of drainage basins. *JGR Earth Surface* 117: F02028.
- Phillips JD (1991) Fluvial sediment budgets in the North Carolina Piedmont. *Geomorphology* 4: 231–241.
- Pongratz J, Reick CH, Raddatz T et al. (2009) Effects of anthropogenic land cover change on the carbon cycle of the last millennium. *Global Biogeochemical Cycles* 23: GB4001.
- Quinton JN, Govers G, Van Oost K et al. (2010) The impact of agricultural soil erosion on biogeochemical cycling. *Nature Geosci* 3: 311–314.
- Rommens T, Verstraeten G, Bogman P et al. (2006) Holocene alluvial sediment storage in a small river catchment in the loess area of central Belgium. *Geomorphology* 77: 187–201.
- Rommens T, Verstraeten G, Peeters I et al. (2007) Reconstruction of late-Holocene slope and dry valley sediment dynamics in a Belgian loess environment. *The Holocene* 17: 777–788.
- Rommens T, Verstraeten G, Poesen J et al. (2005) Soil erosion and sediment deposition in the Belgian loess belt during the Holocene: Establishing a sediment budget for a small agricultural catchment. *The Holocene* 15: 1032–1043.
- Ruddiman WF (2007) The early anthropogenic hypothesis: Challenges and Responses. *Reviews of Geophysics* 45. Available at: <https://agupubs.onlinelibrary.wiley.com/doi/epdf/10.1029/2006RG000207>.
- Saito Y, Yang Z and Hori K (2001) The Huanghe (Yellow River) and Changjiang (Yangtze River) deltas: A review on their characteristics, evolution and sediment discharge during the Holocene. *Geomorphology* 41: 219–231.
- Stallard RF (1998) Terrestrial sedimentation and the carbon cycle: Coupling weathering and erosion to carbon burial. *Global Biogeochemical Cycles* 12: 231–257.
- Stocker BD, Strassmann K and Joos F (2011) Sensitivity of Holocene atmospheric CO<sub>2</sub> and the modern carbon budget to early human land use: Analyses with a process-based model. *Biogeosciences* 8: 69–88.
- Syvitski JPM, Vörösmarty CJ, Kettner AJ et al. (2005) Impact of humans on the flux of terrestrial sediment to the global coastal ocean. *Science* 308: 376–380.
- Trimble SW (1981) Changes in sediment storage in the Coon Creek Basin, Driftless Area, Wisconsin, 1853 to 1975. *Science* 214: 181–183.
- Trimble SW (1999) Decreased rates of alluvial sediment storage in the Coon Creek Basin, Wisconsin, 1975–93. *Science* 285: 1244–1246.
- van Hooff PPM and Jungerius PD (1984) Sediment source and storage in small watersheds on the Keuper marls in Luxembourg, as indicated by soil profile truncation and the deposition of colluvium. *CATENA* 11: 133–144.
- Van Oost K, Quine TA, Govers G et al. (2007) The impact of agricultural soil erosion on the global carbon cycle. *Science* 318: 626–629.
- Van Oost K, Verstraeten G, Doetterl S et al. (2012) Legacy of human-induced C erosion and burial on soil–atmosphere C exchange. *Proceedings of the National Academy of Sciences* 109: 19492–19497.
- Van Rompaey AJJ, Govers G, Van Hecke E et al. (2001) The impacts of land use policy on the soil erosion risk: A case study in central Belgium. *Agriculture, Ecosystems & Environment* 83: 83–94.
- Vanacker V, von Blanckenburg F, Govers G et al. (2007) Restoring dense vegetation can slow mountain erosion to near natural benchmark levels. *Geology* 35: 303–306.
- Verstraeten G and Prosser IP (2008) Modelling the impact of land-use change and farm dam construction on hillslope sediment delivery to rivers at the regional scale. *Geomorphology* 98: 199–212.
- Verstraeten G, Rommens T, Peeters I et al. (2009) A temporarily changing Holocene sediment budget for a loess-covered catchment (central Belgium). *Geomorphology* 108: 24–34.
- Wang S, Fu B, Piao S et al. (2016) Reduced sediment transport in the Yellow River due to anthropogenic changes. *Nature Geoscience* 9: 38–41.
- Wang Z, Hoffmann T, Six J et al. (2017) Human-induced erosion has offset one-third of carbon emissions from land cover change. *Nature Climate Change* 7: 345–349.
- Wang Z, Van Oost K, Lang A et al. (2014) The fate of buried organic carbon in colluvial soils: A long-term perspective. *Biogeosciences* 11: 873–883.
- Waters CN, Zalasiewicz J, Summerhayes C et al. (2016) The Anthropocene is functionally and stratigraphically distinct from the Holocene. *Science* 351: aad2622.
- Webb RS and Rosenzweig CE (1993) Specifying land surface characteristics in general circulation models: Soil profile data set and derived water-holding capacities. *Global Biogeochemical Cycles* 7: 97–108.
- Wilkinson BH and McElroy BJ (2007) The impact of humans on continental erosion and sedimentation. *Geological Society of America Bulletin* 119: 140–156.
- Wolf D and Faust D (2013) Holocene sediment fluxes in a fragile loess landscape (Saxony, Germany). *CATENA* 103: 87–102.
- Yoo K, Mudd SM, Sanderman J et al. (2009) Spatial patterns and controls of soil chemical weathering rates along a transient hillslope. *Earth and Planetary Science Letters* 288: 184–193.
- Yue Y, Ni J, Ciais P et al. (2016) Lateral transport of soil carbon and land–atmosphere CO<sub>2</sub> flux induced by water erosion in China. *Proceedings of the National Academy of Sciences* 113: 6617–6622.
- Zhao J, Van Oost K, Chen L et al. (2016) Moderate topsoil erosion rates constrain the magnitude of the erosion-induced carbon sink and agricultural productivity losses on the Chinese Loess Plateau. *Biogeosciences* 13: 4735–4750.